Low-loss 3D-laser-written mid-infrared LiNbO₃ depressed-index cladding waveguides for both TE and TM polarizations

HUU-DAT NGUYEN,[1] AIRÁN RÓDENAS,[1,2,*] JAVIER R. VÁZQUEZ DE ALDANA,[3] GUILLERMO MARTÍN,[4] JAVIER MARTÍNEZ,[1] MAGDALENA AGUILÓ,[1] MARIA CINTA PUJOL,[1] AND FRANCESC DÍAZ[1]

[1]*Física i Cristal·lografía de Materials i Nanomaterials (FiCMA-FiCNA-EMAS), Departament de Química Física i Inorgànica, Universitat Rovira i Virgili, (URV), 43007, Tarragona, Spain*
[2]*Istituto di Fotonica e Nanotecnologie - Consiglio Nazionale delle Ricerche, Piazza Leonardo da Vinci, 32, I-20133 Milano, Italy*
[3]*Grupo de Investigación en Aplicaciones del Láser y Fotónica (ALF-USAL), Facultad de Ciencias, Universidad de Salamanca, E-37008 Salamanca, Spain*
[4]*UJF-Grenoble 1 / CNRS-INSU, Institut de Planétologie et d'Astrophysique de Grenoble (IPAG), Grenoble, France*
*arodenas@gmail.com

Abstract: We report mid-infrared LiNbO₃ depressed-index microstructured cladding waveguides fabricated by three-dimensional laser writing showing low propagation losses (~1.5 dB/cm) at 3.68 µm wavelength for both the transverse electric and magnetic polarized modes, a feature previously unachieved due to the strong anisotropic properties of this type of laser microstructured waveguides and which is of fundamental importance for many photonic applications. Using a heuristic modeling-testing iteration design approach which takes into account cladding induced stress-optic index changes, the fabricated cladding microstructure provides low-loss single mode operation for the mid-IR for both orthogonal polarizations. The dependence of the localized refractive index changes within the cladding microstructure with post-fabrication thermal annealing processes was also investigated, revealing its complex dependence of the laser induced refractive index changes on laser fabrication conditions and thermal post-processing steps. The waveguide modes properties and their dependence on thermal post-processing were numerically modeled and fitted to the experimental values by systematically varying three fundamental parameters of this type of waveguides: depressed refractive index values at sub-micron laser-written tracks, track size changes, and piezo-optic induced refractive index changes.

References and links

1. R. R. Thomson, S. Campbell, I. J. Blewett, A. K. Kar, and D. T. Reid, "Optical waveguide fabrication in z-cut lithium niobate (LiNbO₃) using femtosecond pulses in the low repetition rate regime," Appl. Phys. Lett. **88**(11), 111109 (2006).
2. R. Osellame, M. Lobino, N. Chiodo, M. Marangoni, G. Cerullo, R. Ramponi, H. T. Bookey, R. R. Thomson, N. D. Psaila, and A. K. Kar, "Femtosecond laser writing of waveguides in periodically poled lithium niobate preserving the nonlinear coefficient," Appl. Phys. Lett. **90**(24), 241107 (2007).
3. J. Burghoff, C. Grebing, S. Nolte, and A. Tünnermann, "Efficient frequency doubling in femtosecond laser-written waveguides in lithium niobate," Appl. Phys. Lett. **89**(8), 081108 (2006).
4. R. He, Q. An, Y. Jia, G. R. Castillo-Vega, J. R. Vázquez de Aldana, and F. Chen, "Femtosecond laser micromachining of lithium niobate depressed cladding waveguides," Opt. Mater. Express **3**(9), 1378–1384 (2013).
5. J. Burghoff, S. Nolte, and A. Tünnermann, "Origins of waveguiding in femtosecond laser structured LiNbO₃," Appls. Phys. A Mater. Sci. Process. **89**(1), 127–132 (2007).

6. H. Karakuzu, M. Dubov, and S. Boscolo, "Control of the properties of micro-structured waveguides in lithium niobate crystal," Opt. Express **21**(14), 17122–17130 (2013).
7. R. S. Weis and T. K. Gaylord, "Lithium niobate: Summary of physical properties and crystal structure," Appl. Phys., A Mater. Sci. Process. **37**(4), 191–203 (1985).
8. S. Heidmann, N. Courjal, and G. Martin, "Double polarization active Y junctions in the L band, based on Ti:LiNbO₃ lithium niobate waveguides: polarization and contrast performances," Opt. Lett. **37**(16), 3318–3320 (2012).
9. G. Martin, S. Heidmann, J.-Y. Rauch, L. Jocou, and N. Courjal, "Electro-optic fringe locking and photometric tuning using a two-stage Mach-Zehnder lithium niobate waveguide for high-contrast mid-infrared interferometry," Opt. Eng. **53**(3), 034101 (2014).
10. F. Thomas, S. Heidmann, M. de Mengin, N. Courjal, G. Ulliac, A. Morand, P. Benech, E. Le Coarer, and G. Martin, "First Results in Near and Mid IR Lithium Niobate-Based Integrated Optics Interferometer Based on SWIFTS-Lippmann Concept," J. Lightwave Technol. **32**(22), 3736–3742 (2014).
11. D. Jaque, E. Cantelar, and G. Lifante, "Lattice micro-modifications induced by Zn diffusion in Nd:LiNbO₃ channel waveguides probed by Nd³⁺ confocal micro-luminescence," Appl. Phys. B **88**(2), 201–204 (2007).
12. D. Castaldini, P. Bassi, S. Tascu, P. Aschieri, M. P. De Micheli, and P. Baldi, "Soft-proton-exchange tapers for low insertion-loss LiNbO₃ devices," J. Lightwave Technol. **25**(6), 1588–1593 (2007).
13. G. B. Montanari, P. De Nicola, S. Sugliani, A. Menin, A. Parini, A. Nubile, G. Bellanca, M. Chiarini, M. Bianconi, and G. G. Bentini, "Step-index optical waveguide produced by multi-step ion implantation in LiNbO₃," Opt. Express **20**(4), 4444–4453 (2012).
14. S. Juodkazis, V. Mizeikis, and H. Misawa, "Three-dimensional microfabrication of materials by femtosecond laser for photonics applications," J. Appl. Phys. **106**(5), 051101 (2009).
15. S. Nolte, M. Will, J. Burghoff, and A. Tünnermann, "Femtosecond waveguide writing: a new avenue to the three-dimensional integrated optics," Appl. Phys., A Mater. Sci. Process. **77**(1), 109–111 (2003).
16. R. Osellame, G. Cerullo, and R. Ramponi, eds., Femtosecond Laser Micromachining: Photonic and Microfluidic Devices in Transparent Materials, Topics in Applied Physics 123 (Springer-Verlag, 2012).
17. A. Ródenas, G. Zhou, D. Jaque, and M. Gu, "Direct laser writing of three-dimensional photonic structures in Nd:yttrium aluminum garnet laser ceramics," Appl. Phys. Lett. **93**(15), 151104 (2008).
18. A. Ródenas, G. A. Torchia, G. Lifante, E. Cantelar, J. Lamela, F. Jaque, L. Roso, and D. Jaque, "Refractive index change mechanisms in femtosecond laser written ceramic Nd:YAG waveguides: micro-spectroscopy experiments and beam propagation calculations," Appl. Phys. B **95**(1), 85–96 (2009).
19. A. Ródenas, "Direct femtosecond laser writing of 3D photonic structures in rare-earth doped lithium niobate," (Universidad Autónoma de Madrid, 2009).
20. H. D. Nguyen, A. Ródenas, J. R. Vázquez de Aldana, J. Martínez, F. Chen, M. Aguiló, M. C. Pujol, and F. Díaz, "Heuristic modelling of laser written mid-infrared LiNbO₃ stressed-cladding waveguides," Opt. Express **24**(7), 7777–7791 (2016).
21. A. Rodenas and A. K. Kar, "High-contrast step-index waveguides in borate nonlinear laser crystals by 3D laser writing," Opt. Express **19**(18), 17820–17833 (2011).
22. H. Liu, Y. Jia, J. R. Vázquez de Aldana, D. Jaque, and F. Chen, "Femtosecond laser inscribed cladding waveguides in Nd:YAG ceramics: Fabrication, fluorescence imaging and laser performance," Opt. Express **20**(17), 18620–18629 (2012).
23. J. Hu and C. R. Menyuk, "Understanding leaky modes: slab waveguide revisited," Adv. Opt. Photonics **1**(1), 58–106 (2009).
24. Q. An, Y. Ren, Y. Jia, J. R. Vázquez de Aldana, and F. Chen, "Mid-infrared waveguides in zinc sulfide crystal," Opt. Mater. Express **3**(4), 466–471 (2013).
25. A. Ródenas, L. M. Maestro, M. Ramirez, G. A. Torchia, L. Roso, F. Chen, and D. Jaque, "Anisotropic lattice changes in femtosecond laser inscribed Nd³⁺:MgO:LiNbO₃ optical waveguides," J. Appl. Phys. **106**(1), 013110 (2009).
26. B. McMillen and Y. Bellouard, "On the anisotropy of stress-distribution induced in glasses and crystals by non-ablative femtosecond laser exposure," Opt. Express **23**(1), 86–100 (2015).
27. H. Karakuzu, M. Dubov, S. Boscolo, L. A. Melnikov, and Y. A. Mazhirina, "Optimisation of microstructured waveguides in z-cut LiNbO₃ crystals," Opt. Mater. Express **4**(3), 541–552 (2014).
28. R. He, Q. An, J. R. Vázquez de Aldana, Q. Lu, and F. Chen, "Femtosecond-laser micromachined optical waveguides in Bi₄Ge₃O₁₂ crystals," Appl. Opt. **52**(16), 3713–3718 (2013).
29. D. E. Zelmon, D. L. Small, and D. Jundt, "Infrared corrected Sellmeier coefficients for congruently grown lithium niobate and 5 mol.% magnesium oxide –doped lithium niobate," J. Opt. Soc. Am. B **14**(12), 3319–3322 (1997).
30. S. Gross, N. Jovanovic, A. Sharp, M. Ireland, J. Lawrence, and M. J. Withford, "Low loss mid-infrared ZBLAN waveguides for future astronomical applications," Opt. Express **23**(6), 7946–7956 (2015).
31. J. Martínez de Mendívil, D. Sola, J. R. Vázquez de Aldana, G. Lifante, A. H. de Aza, P. Pena, and J. I. Peña, "Ultrafast direct laser writing of cladding waveguides in the 0.8CaSiO₃-0.2Ca₃(PO₄)₂ eutectic glass doped with Nd³⁺ ions," J. Appl. Phys. **117**(4), 043104 (2015).
32. A. Benayas, D. Jaque, B. McMillen, and K. P. Chen, "Thermal stability of microstructural and optical modifications induced in sapphire by ultrafast laser filamentation," J. Appl. Phys. **107**(3), 033522 (2010).

33. J. Burghoff, H. Hartung, S. Nolte, and A. Tünnermann, "Structural properties of femtosecond laser-induced modifications in LiNbO₃," Appl. Phys., A Mater. Sci. Process. **86**(2), 165–170 (2006).

34. A. M. Prokhorov and Y. S. Kuz'minov, *Physics and Chemistry of Crystalline Lithium Niobate* (Taylor & Francis Ltd, 1990).

35. A. Benayas, W. F. Silva, C. Jacinto, E. Cantelar, J. Lamela, F. Jaque, J. R. Vázquez de Aldana, G. A. Torchia, L. Roso, A. A. Kaminskii, and D. Jaque, "Thermally resistant waveguides fabricated in Nd:YAG ceramics by crossing femtosecond damage filaments," Opt. Lett. **35**(3), 330–332 (2010).

1. Introduction

Lithium niobate (LiNbO₃) has been established as a versatile material for integrated electro-optic devices and nonlinear optical applications due to its high electro-optical and non-linear coefficients, its well-developed industrial manufacturing quality, and its large transparency window from the UV to the mid-IR [1–4]. The large developments on LiNbO₃ devices for the telecom range in the last three decades enable LiNbO₃ crystals to be a promising material for the mid-IR photonics as well, with wide applications in chemical and bio-medical fields, in atmospheric research, high-resolution on-chip vibrational spectroscopy, and astrophotonic instrumentation [2–10]. Conventionally, lithographic techniques such as ion in-diffusion, ion implantation and soft proton exchange have been employed to manufacture optical waveguide structures in LiNbO₃ [11–13]. However, the lithographic approach is limited to a two-dimensional (2D) layout which does not allow to fully exploit three-dimensional circuit architectures, which are compulsory for multi-channel beam combination, in particular in the field of astrophotonics and stellar interferometry. The direct femtosecond (fs) laser writing has emerged as a versatile and efficient tool which enables the three-dimensional (3D) laser writing (3DLW) of complex waveguide designs within a short timescale of minutes [14–16]. However, LiNbO₃ still poses various serious challenges for the 3DLW technique to be reliable and efficient for photonic fabrication: its birefringence induces aberration of the writing focal volume when using high numerical aperture lenses, and its photo-refractive, piezo-optic and non-linear properties further complicate the 3DLW fabrication process to a very high degree [2,7].

The tight focusing of fs near-IR laser pulses inside the host material are known to induce a non-linear absorption which results in a spatially localized lattice change in the sub-micron scale [14–21]. The structural changes involve electronic defects or lattice defects, so that in general a change in the material involves modified refractive and absorptive properties through a change in the complex refractive index ($\Delta n^* = \Delta n + i\Delta\kappa$, where Δn is the change in the real part of the index of refraction and $\Delta\kappa$ is the change in the extinction coefficient). It is important to note that index changes can vary significantly if measured at the visible, near-IR or mid-IR ranges, since the material polarizability and defects absorption in these ranges have distinctive origins. However, these effects are difficult to know due to the difficulty in measuring index changes in nanostructured volumes at different wavelengths, and only a few works have reported on the dispersion of Δn at different wavelengths in laser written waveguides [21]. In general, two fundamental types of index modification Δn have been reported with the 3DLW technique in LiNbO₃, which are the so called Type I (increased refractive index at the laser writing focal volume) and Type II (negative index change at the laser writing focal volume, and strong stress field surrounding the track due to lattice amorphization and defect generation, involving collateral piezo-optic index changes) [1,3]. Depressed-index cladding waveguides, hereafter CLWs, are normally written by drawing two-dimensional tubular structures in the regime for Type II index changes, and which therefore act as depressed cladding (see inset in Fig. 1). The guiding properties depend on the magnitude of the negative Δn change produced at the written tracks, and on the size and spatial width of the cladding arrangement [20]. The final refractive index profiles of a whole cladding structure are dependent on (1) the local Δn at the modified tracks and on (2) the anisotropic piezo-optic index changes in the surroundings of tracks, which strongly depend on

the chosen 3DLW parameters: i.e. pulse duration, pulse energy, repetition rate, scanning speed, wavelength, polarization, and focusing optics.

Recently, the mid-IR refractive index profile of 3DLW LiNbO$_3$ microstructured cladding waveguides was reported for the first time [20]. The refractive index estimations were performed by means of a combination of experimental characterizations and detailed finite element method (FEM) based simulation models of the microstructures taking into account both refractive index changes due to direct fs laser modification and also the stress-induced birefringent index changes [20]. However, single mode optical guiding was only demonstrated for TE horizontally polarized light and not for TM polarization, due to the strong anisotropy of the cladding structures, this implying that the Δn profiles of the waveguides for TM modes could not be assessed, and also no guiding for both TE/TM light could be achieved. Moreover, the demonstrated propagation losses for single mode TE waveguides was of 2.9 dB/cm, far from being low losses. There exists therefore a fundamental bottleneck for obtaining CLWs in LiNbO$_3$ for mid-IR applications, capable of single mode guiding with low propagation losses for both orthogonal polarizations. Not in vain, single mode LiNbO$_3$ CLWs with propagation losses (PLs) lower than ~3 dB/cm at wavelength longer than 3 μm are still to be demonstrated [6,20–27]. In the search for improving the optical performance of CLWs, thermal treatments have been also performed to remove the anisotropic micro-stress fields induced during the laser writing process [4,27,28], since this induced stress is considered as one of the major factors causing the birefringent behavior of the CLWs. However, a clear understanding of the changes in waveguide profiles under different annealing conditions is also still missing, and 3DLW mid-IR LiNbO$_3$ single mode CLWs in particular have not yet been studied in combination with post-fabrication annealing treatments, mainly due to the high difficulties in assessing refractive index changes in this long wavelength range.

The goal of this work is to further understand the micro- and nano-structural refractive index changes, which take place in 3DLW LiNbO$_3$ CLWs, with the aim of achieving single mode low-loss propagation for both TE/TM polarizations. By means of refining the microstructural designs of CLWs, and studying their guiding properties both in as-fabricated samples and annealed samples, we infer how the sub-micron laser written tracks change in both size and index of refraction, and also how the stress-fields are reduced as a function of annealing temperature and time. Results reveal that by performing thermal annealings until a cladding design dependent temperature, single mode guiding for both polarizations can be achieved, with a minimum obtained propagation losses of 1.25 dB/cm and 1.79 dB/cm for TM and TE polarizations, respectively.

2. Materials and technical details

2.1 Design and numerical modelling

Cladding waveguide design and numerical analysis were done by using a finite element computational method (FEM hereafter) using commercial COMSOL package, and which takes into account both constant refractive index changes inside the laser written tracks and its surrounding piezo-optic index changes, supposing a thermal expansion of the laser written tracks, as previously reported [20]. The micrometric volume changes induced by the localized femtosecond pulse ionization inside LiNbO$_3$ were simulated with a 2D thermal expansion model which yields the stress distribution in the expanded track surroundings. The inside of laser written tracks is approximated to be constant and have a negative index change. The studied 2D stress fields are responsible for anisotropic refractive index changes surrounding the laser-modified low-index tracks due to the piezo-optic effect. Once a full cladding waveguide refractive index profile is obtained, the mode analysis is performed with an electromagnetic-wave frequency-domain model. All simulations are calculated for a free space wavelength of 3.68 μm where ordinary and extraordinary index values of LiNbO$_3$ are $n_{y(o)} = 2.1309$ and $n_{z(e)} = 2.0700$, respectively [29]. The numerical mode calculation gives the

near-field distributions of the guided waveguide modes and their corresponding effective indices which are used to obtain the theoretical mode field diameters (MFDs) and propagation losses (PLs), respectively (for further details see [20]).

Previously reported single-mode mid-IR waveguides [20] were fabricated with a core of 40 μm and cladding width of 10 μm (vertical size of a single track) and were experimentally found to support guiding only for TE polarized light with high PLs of around ~3 dB/cm [20]. Increasing the core diameter and the width of the cladding structure is known to result in reduction of PLs of the fundamental mode, although avoiding the excitation of higher order modes for any polarization can be difficult [20,27,30]. Therefore, in this work the waveguides are designed with a two-fold widened cladding arrangement consisting of two rings of tracks, with a core diameter of 50 μm (hereafter CLW2R) aimed to offer low-loss optical guiding for both polarizations with minimized birefringent effect. In order to get an initial approximation, the waveguide design and computation take as starting parameters the refractive index contrast and induced-stress magnitudes obtained in our previous study [20], and develops towards better optical performances using a minimized number of tracks given the double-ring structure. The initial cladding structure consists of 174 laser-written tracks spaced by 2 μm, forming an unmodified circular core of 50 μm in diameter (see inset of Fig. 1). However, due to aberration effects of the focal volume inside $LiNbO_3$, 117 extra tracks were added to the model replicating the experimentally observed appearance of secondary focal points of the writing laser beam around 8 μm above the primary focus and for focusing depths higher than 300 μm. By means of atomic force microscopy (AFM) and scanning electron microscopy (SEM) imaging, the laser-inscribed tracks were measured to have elliptical shapes with a length of 7 μm along the incident direction of the laser beam (z-axis, vertical) and a width of 300 nm along the perpendicular direction (y-axis, horizontal). The measured sizes of the extra tracks were around 66% of the primary tracks. The fabricated cladding layer is almost uniform with an approximate width of 16 μm except in its the lower part where it is thicker due to the extra tracks created by the focal volume aberrations.

Following previous works [18], it is expected that under the processes of thermal annealing the laser-modified depressed-index tracks will reduce in size and in refractive index change magnitude with respect to the bulk, and the stress fields will be relaxed. These microstructural changes will result in complex changes of optical guiding performance, since depressed index tracks conform the cladding and the stress-induced index changes reinforce or weaken it depending on the sign of the piezo-optic induced refractive index change. The study of these three variables (depressed-refractive indices, stress-induced refractive indices and track dimensions) is therefore carried out for each different thermal annealing process, by matching both the theoretical MFD and PL values to the experimental results (discussed in section §3.2), this allowing to unveil how these mid-IR waveguides change their properties with annealing temperatures above 573 K (300°C).

2.2 Femtosecond laser fabrication

The laser fabrication involves the transversal inscription of tracks to construct a depressed-Δn circular array which supports leaky modes along the tubular channel [23]. Geometrical coordinates of each individual track were extracted from the 2D design and loaded to a script used in the laser inscription process. Trial of writing single tracks was initially conducted in order to specify the track sizes as a function of laser energy and focusing depth.

The femtosecond laser beam used for waveguide fabrication was linearly polarized along the y-axis of the crystal (perpendicular to the scanning direction). A 90° rotation of the polarization direction did not produce significant differences in the fabricated structures. Such independence, to our knowledge, is due to the fact that the propagation direction of the femtosecond laser is along the z-axis of the crystal (z-cut sample) and thus the polarization is mainly contained in the isotropy plane.

The 3D laser writing (3DLW) was processed along the z-axis of a z-cut LiNbO$_3$ sample with dimensions of $20(x) \times 10(y) \times 1(z)$ mm^3 (include the commercial source of the crystal). All faces of the sample were optically polished with high quality before starting the fabrication processes. The optical fabrication setup includes a Ti:Sapphire regenerative amplified laser system (Spitfire and Tsunami systems, Spectra-Physics) which produces linearly-polarized pulses of ~120 fs duration, with a repetition rate of 1 kHz at a central wavelength of 795 nm. A series of pulse energies were adjusted by using a calibrated neutral density filter, a half-wave plate and a linear polarizer. A high-resolution three-axis motorized stage was used to mount the sample and precisely move the positions corresponding to the programmed script. A microscope objective (40 × , NA = 0.65) was used to focus the laser beam through the xy plane of the sample at a central depth of 300 µm. The laser scanning direction was along the long dimension (20 mm, x-axis) of the crystal. Separation of the tracks in the y-direction was fixed to 2 µm. Laser polarization was kept perpendicular to the scanning direction. In the first set of waveguides, a series of eight pulse energy values (0.84 µJ to 2.31 µJ, with increment of 0.21 µJ) was performed along with a fixed scan velocity of 750 µm/s. The second set of waveguides was done with three values of pulse energy (0.84 µJ to 1.68 µJ, with increment of 0.42 µJ) and a fixed scan velocity of 500 µm/s.

2.3 Optical waveguide characterization

Microscope optical imaging of the cladding structure was done with a blue-LED confocal optical microscope (Sensofar PLµ 2300). In order to obtain high resolution images of the tracks, SEM characterisation was also performed. In addition, AFM was also used to investigate the nanometric widths of the single tracks, after the sample was slightly chemically etched with nitric acid at room temperature for 30 seconds so that the laser-damage tracks were revealed.

The waveguides were characterised at the wavelength of 3.68 µm with a linearly polarized interband cascade laser. The collimated laser beam was directed with two mirrors to undergo a change in height so that its final polarization was linear at 45° with respect to both the vertical and horizontal polarization axes. Two linear polarizers were then used to select either horizontal (TE) or vertical (TM) polarizations, one polarizer before the input lens, and the second after the output lens. A micro-positioning stage with 5-axis manual microcontrollers was used to align the sample. Input light was launched in the waveguides with an aspheric lens of 0.18NA, and the waveguides output modes near fields were imaged with a FLIR SC700 mid-IR camera and an aspheric lens with 0.56 NA. A pinhole was placed before the input lens so as to finely adjust the beam diameter and optimize the input coupling into waveguides. The coupling efficiency was calculated by means of overlap integral between the optimal input spot size and each waveguide output mode. PLs were calculated by subtracting the input coupling losses and double Fresnel losses to the measured total insertion losses at the optimal input spot size.

2.4 Thermal annealing

Thermal treatments of the waveguides were performed in a furnace with open-air condition. A series of seven annealing processes at different maximum temperatures was carried out. The first annealing was done at a maximum temperature of 573 K (300°C) for 3 hours, with a 2 K per minute ramp for heating up and cooling down. The same processes were repeated with increasing maximum temperatures of 773, 873, 973, 1073, 1123 and 1173 K (900°C). Since the annealing was repeatedly done on the same sample, the final result is an accumulation of heat treatments from all the preceding processes. The sample was analysed by SEM and the waveguides were fully characterized after each annealing step.

3. Results

3.1 Mid-IR optical guiding properties of waveguides

All propagation losses obtained from the guiding characterization of as-fabricated (no annealings) are listed in Table 1 and shown in Fig. 1.

Group A consists of 8 waveguides fabricated with a fixed scan speed of 750 μm/s (hereafter named 750_wg#) and different pulse energy values chosen within the range that provided enough power to cause depressed-Δn damage and observable guiding, and did not induce cracks within the CLWs. Waveguide 750_wg5 had a surface damage and therefore could therefore not be precisely characterized. Group B has three waveguides fabricated with three different pulse energies and a fixed scan velocity of 500 μm/s (hereafter 500_wg#). All the waveguides showed guiding for both TE and TM modes. However, while all CLWs were observed to be single mode for TM polarized light, multimode guiding was observed for TE polarization. This behavior shows how strong is the role of the anisotropic stress-induced Δn profiles.

Table 1. Propagation losses of the CLW2Rs fabricated with different laser conditions

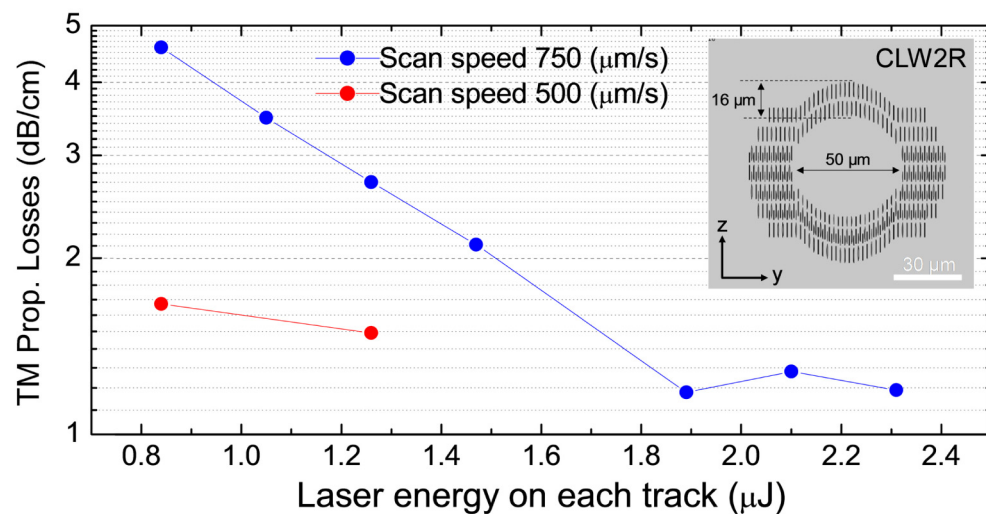|	Group A 750 μm/s scan velocity								Group B 500 μm/s scan velocity		
	750_ wg1	750_ wg2	750_ wg3	750_ wg4	750_ wg5	750_ **wg6**	750_ wg7	750_ **wg8**	500_ wg1	500_ wg3	500_ wg5
Pulse energy (μJ)	0.84	1.05	1.26	1.47	1.68	1.89	2.10	2.31	0.84	1.26	1.68
TE-PLs (dB/ cm)	MM	MM	MM	MM	MM	MM	MM	MM	MM	MM	MM
TM-PLs (dB/cm)	4.59	3.48	2.70	2.11	x	**1.18**	1.28	**1.19**	1.67	1.49	MM

MM: multimode; x: not guided

Fig. 1. Propagation losses for TM mode of CLW2Rs fabricated by different pulse energies and scanning velocities. Lines joining experimental points are added only as visual help.

Since the waveguides are multimode for the TE polarized light, PLs were not measured for this case, since our goal is to have single mode waveguides and characterize their losses. For the case of TM polarized light, a clear trend is observed that the higher the pulse energies by which the waveguides were fabricated, the better guiding performance they have in terms of lower PLs, however this at the cost of having increasing number of modes for the

orthogonal polarization (TE). As it can be expected, this could be due to the increasing Δn magnitude of the depressed cladding tracks. The lowest PL of 1.19 dB/cm was obtained by the waveguide 750_wg8 written by the highest laser pulse energy of 2.31 μJ and scanning speed of 750 μm/s. Waveguides fabricated with lower scanning speeds were measured to have lower losses (Fig. 1. Red line), although no CLWs could be fabricated at pulse energies above 1.3 μJ due to lack of space within the LiNbO$_3$ sample. Lower writing speed produce a larger pulse overlap along the scanning direction which in turn results in more homogeneous depressed index tracks, therefore producing a better confining region. However, this is also at the cost of increased fabrication times.

3.2. Guiding performance of waveguides under heat treatments

The main goal of treating the waveguides with thermal annealing was to reduce the level of the anisotropic stress which might benefit the optical performance for one polarization and deteriorate the other, due to the fact that piezo-optic induced refractive index changes have opposite sign for orthogonal polarizations. Improvements of optical properties with the help of heat treatments have been reported for laser-written cladding waveguides on different materials, although no work has yet been performed for the mid-infrared range. He et al. have demonstrated a 30% decrease of PLs when CLWs on bismuth germanium oxide (BGO) crystal were treated at 533K for 2 hours [28]. However, the BGO waveguides increased the losses at the annealing temperature of 633K, and started to disappear at higher temperatures. Another work was done with the study of CLWs on neodymium doped wollastonite tricalcium phosphate glass as a function of annealing temperature [31]. The transmitted optical power of these glass CLWs was improved as a factor of 3 when treated at up to 873K. With the heat treatment higher than 923K, a dramatic increase of PLs was observed. For the case of CLWs on LiNbO$_3$, single mode CLWs were enhanced in transmission with PLs from 5.3 to 4.3 dB/cm for 4 μm wavelength by annealing at 533K for 1 hour [4]. It should be noted however, that neither of these works was performed for mid-IR light, and therefore the effects and dependences of high temperature annealing processes with the material refractive index changes can be different to our present analysis.
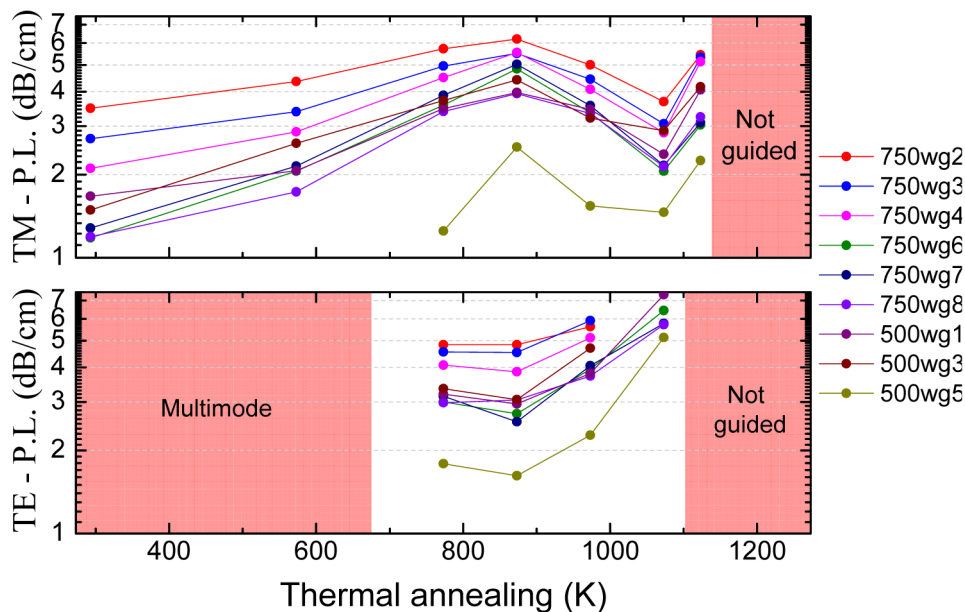

Fig. 2. Waveguide performances with respect to different heat treatments. PLs of the waveguides for TM polarization (upper graph) and TE polarization (lower graph). Lines joining experimental points are added only as visual help.

In our work, the behavior of this type of waveguide was revealed to be complicated when studied with a broad range of annealing temperatures (573K to 1173K). The initially non-annealed waveguides clearly showed a strong birefringent characteristic with mono-mode behavior for TM polarized light, while multimode was observed for TE light. The annealing treatment helped to clean the higher order modes of the TE polarization and left the CLW2Rs to have single mode behavior after sequential heating treatments of 573 and 773K for 3 hours each (see Fig. 2, lower graph). With higher annealing temperatures and longer annealing times, the PLs of these TE modes steadily increased. The same trend happened to all the waveguides, and all stopped guiding light when annealed at peak temperature of higher than 1073K. Here, the waveguide 750_wg1 was not included in the figure due to an accidental break during a manual handling of the sample.

For TM modes, the guiding performance was deteriorated during the first heat treatments of 573, 773 and 873 K, with a clear increase of the PLs (see Fig. 2, upper graph). The trend of PLs was reversed when the temperature was raised to 973K and at the annealing of 1073K the PLs dropped to a bottom which is around the PL levels of the non-annealed waveguides. Consequently, at higher temperature than 1123K the waveguides started to have more losses and vanished after temperature of 1173K. In conclusion, the TM polarized CLWs transmission did not benefit from the annealing treatments. This is a counterintuitive effect, since for TM (vertical) polarization it is well known that a compressive stress between the tracks produces a positive index increase which therefore deteriorates the depressed cladding effect of the tracks microstructure, so that erasing this stress should improve the optical guiding. Contrary to this, the guiding behavior is worsened for TM polarization, so that other microstructural changes must be taking place besides stress field erasure. Overall, as it can be seen in Fig. 2, the CLW 500_wg5, which was fabricated with high pulse energy (1.68 μJ) and slow scan speed (500 μm/s), provides the best optical performance after several heat treatments. This was indeed the only multimode CLW for TM light, so that thermal treatments also allowed to tailor it to be single mode. Details of this waveguide performance will be discussed in section §3.4.

3.3. Heuristic numerical modeling of waveguide properties with respect to thermal treatments

It has been suggested that the effects of the thermal annealing on laser-written waveguides involve several factors: one is a general decrease of induced color centers which increase the absorption of the material within the laser-damaged tracks and its surroundings (although this effect may not be of relevance within the mid-IR range as compared to visible of near-IR ranges where optical centers typically have absorption bands), and the other is a partial erasure of the depressed Δn change [3,5,18,31–33]. Depressed index tracks therefore not only change in optical properties but also in cross-sectional size, becoming smaller as thermal annealings are performed with higher temperatures [18–20]. The residual stress generated during the fs-laser fabrication process is additionally erased, which might be beneficial to the guiding properties of CLW if they are designed as pure depressed refractivd index structures.

In order to closely study these effects, an heuristic simulation model which iteratively feeds from experimental measurements of the mode field diameters and propagation losses (details reported in [20]) was used to estimate the hypothetical changes of the three variables: magnitude and spatial dimensions of the depressed- refractive index regions, and the level of residual stress in their surroundings. The exact values of these variables are strongly dependent on particular conditions of the laser fabrication, so that only once a first test of CLWs is fabricated and characterized under specific 3DLW conditions, modelling has to be done for these CLWs and the use of simulations to optimize the cladding microstructure will only be correct for subsequent CLWs fabricated under exactly the same 3DLW experimental conditions.

A detailed study was performed for the waveguide 750_wg8 which was laser-inscribed with pulse energy of 2.31 μJ and scanning speed of 750 μm/s, for which 8 different pulse energies were tested and therefore further analysis can be undertaken for this writing speed. Before annealing, the 750_wg8 supports monomode guiding for TM polarization and multimode guiding for TE polarization. The fundamental TM mode persisted during annealing of up to 1123K and vanished at higher temperature treatment. In the case of TE mode guiding, higher order modes were cleaned up and the CLW2R started to be single mode after annealed at 773K. The waveguide stopped guiding TE light after 1073K annealing. The measured PLs of these modes are shown in Fig. 3 (solid lines) which resembles the trend of all other waveguides as stated in the previous section §3.2 (Fig. 2). In order to simulate this unique behavior, initial numerical assumptions are made on the three core variables which are used in our model to perform analysis of theoretical guided modes: track sizes, refractive index, and magnitude of induced stress fields surrounding the tracks. The refinement of initial numerical assumptions is then based on optimal matching between theoretical and measured values of MFDs and PLs.
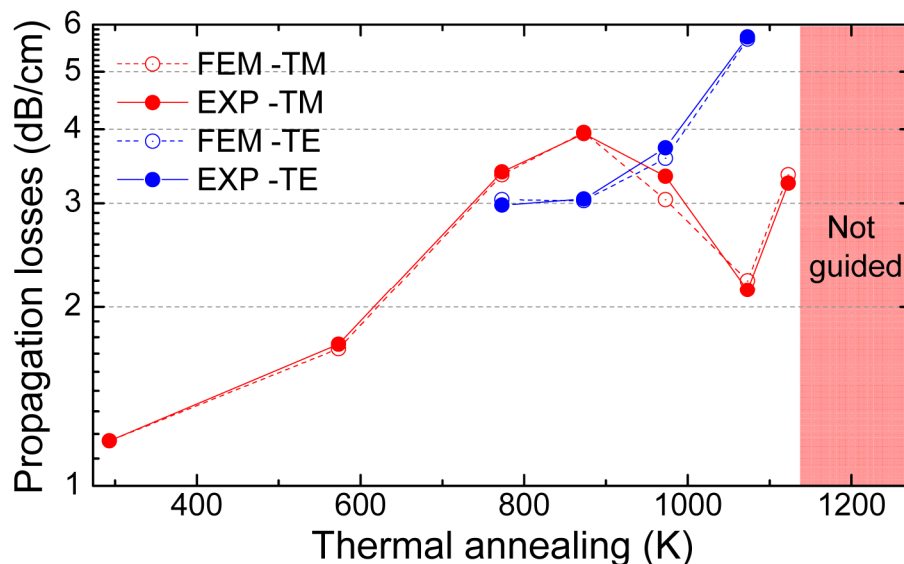

Fig. 3. Theoretical FEM and experimental PL values of the waveguide 750_wg8 versus the thermal annealing temperature. TE (blue graphs) and TM (red graphs) are both considered. The waveguide does not guide after treatment at 1173K. Lines joining experimental points are added only as visual help.

As a starting point, simulation was solved for the as-fabricated waveguide which consists on a double ring tubular microstructure of elliptical tracks with a width of 300 nm and a length of 7 μm (obtained from SEM and AFM characterization). The two other variables to define are the complex index of refraction at laser written tracks (including the extraordinary and ordinary index changes, Δn_z and Δn_y separately) and the value of stress field (σ) induced in the surrounding. In a previous report on mid-IR CLW by authors (using the same 3DLW setup) it was concluded that a maximum compressive stress (σ_y) of ~67 MPa and a complex index change of $\Delta n_y* = -0.008 + i0.0007$ for the single-cladding waveguide (fabricated with low pulse power of 0.6 μJ and writing speed of 700 μm/s) was a best match to experiments for TE polarization (while no TM guiding was observed for a single ring CLW in this previous work) [20]. In the present work, the waveguide has a double-ring wider cladding (see inset of Fig. 1) and was written with a 4 times higher pulse energy of 2.31 μJ, therefore the values of stress and the magnitude of index changes are expected to be higher than those measured in the previous report. Our model however could only be applied for the

polarization for which the CLW is single mode, i.e. TM (vertical) polarization. Several iterations on the CLW modal properties were made with varying numbers of index and stress magnitude.
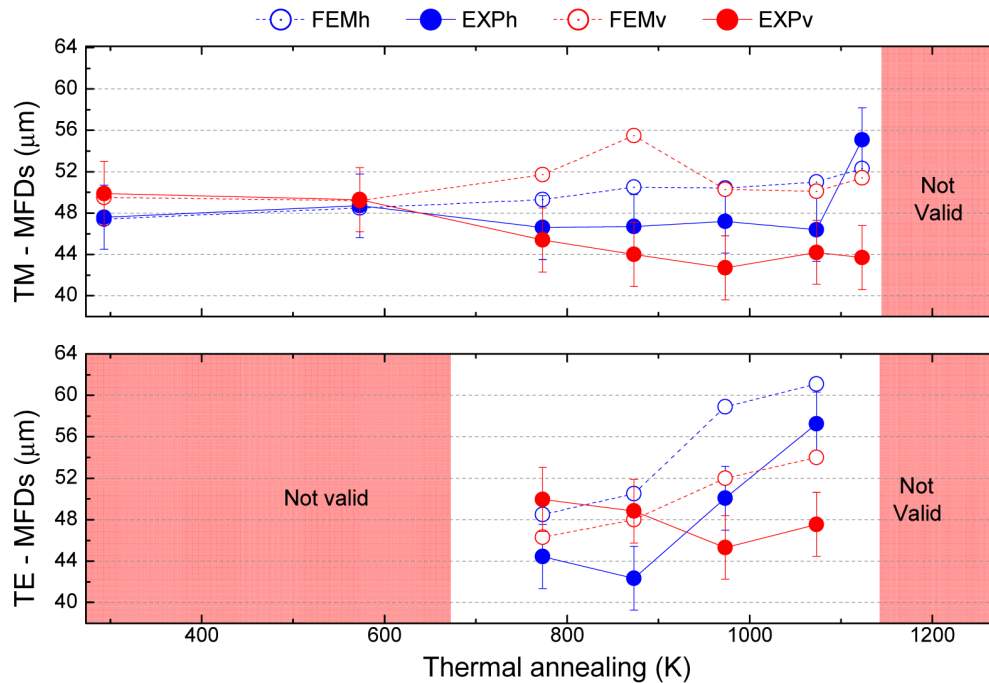

Fig. 4. Theoretical FEM and experimental MFD values of the waveguide 750_wg8 versus the thermal annealing temperature. TE (blue graphs) and TM (red graphs) are both considered. The MFD values are not calculated when either the waveguide is multimode or not guided. The error bar is ± 3 μm. Lines joining experimental points are added only as visual help.

The best matching values of PLs and MFDs were obtained with $n_{e(z)}$ index changes inside tracks of $\Delta n_z^* = -0.022 + i0.007$, which is almost a 3-fold increase with respect to previously reported values of mid-IR CLW. The maximum compressive stress was estimated to be around 180 MPa which is also a 3-fold increase in maximum stress with respect to the value of the single-ring low-pulse energy written CLW. This large increase of the generated stress is also expected as a result of the double-ring cladding. The same procedure was then carried out with all CLWs as a function of the thermal treatments with increasing temperatures. As mentioned above, it is expected that the thermal annealing will facilitate the erasure of the defects which means that the Δn magnitude, the cross-sectional sizes of the tracks and the residual stress levels are expected to decrease. Iterative calculations and comparisons with experiments were therefore made to establish the realistic conditions that best-match experimental measures. As shown in Fig. 3, simulated PLs are almost identical to experimental values. The theoretical MFDs were also matched as best as possible with the experimental values as shown in Fig. 4, within our statistical maximum error of ± 3 μm, which our experimental error in determining the mode near-field diameters, by means of imaging at λ = 3.68 μm wavelength. As shown in Fig. 4, for each polarization for the horizontal (h) and vertical (v) mode near-field cross-section were measured in the experimental modes and simulated modes. As it can be seen a qualitative agreement can be achieved while perfectly matching propagation losses (see Fig. 3).
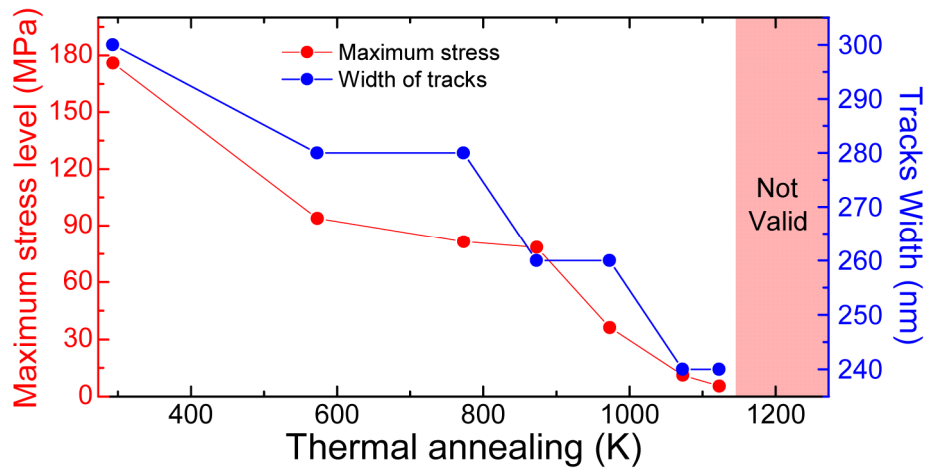
Fig. 5. Width of the laser-damage tracks and the induced stress in the cladding structure under different thermal annealing for waveguide 750_wg8.

3.3.1. Changes of the track dimensions and the induced stress by thermal annealing

Once the best matching of PLs and MFDs was obtained, the resulting changes in tracks dimensions can be studied. The width of the modified tracks shows to experience a linear reduction with increasing annealing temperature (see Fig. 5, blue graph). This was additionally confirmed by SEM and AFM characterisations (results not shown here for the sake of brevity). The width of the tracks is observed to be reduced about a 20% from 300 nm to 240 nm after several annealing steps, and finally a dramatic disappearance was observed at the temperature higher than 1173K, which is close to the melting point of $LiNbO_3$ at 1500K [34]. The vertical length of these tracks also experienced changes, although they were on the nanometer scale which compared to their large length was considered as negligible. The reduction of the residual stress followed the same tendency which fell from 180 MPa down to almost level of 10 MPa and disappeared with the loss of the filaments (Fig. 5, red graph). Previous work had reported these effects on ultrafast laser-written YAG waveguides which addressed similar tendency [35].
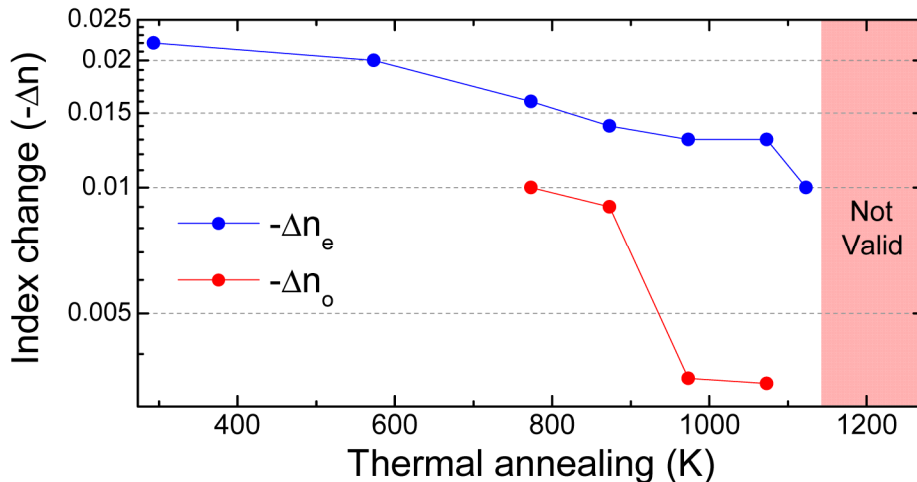

Fig. 6. Index contrast Δn_y (red line) and Δn_z (blue line) between the fs laser-modified tracks and the bulk material of the waveguide 750_wg8 when experienced thermal annealing process.

3.3.2. Changes of the index of refraction

A strongly anisotropic behavior of the two ordinary index Δn_y and extraordinary index Δn_z of laser-modified tracks had been reported for Type I and Type II regimes, under heat treatments of up to 573 K (300°C) and characterized in the visible range (633nm) [33]. Burghoff *et al.* reported no significant change in Type II Δn_y, while the positive Type I Δn_z completely vanished after the laser-written tracks were treated to 573 K [33]. However, our work which has been done on Type II damage tracks at the mid-IR range and under a much wider range of heat treatments (up to 1173K), shows a very different behavior. The decrease of the refractive index contrast between the tracks and the bulk material is displayed in Fig. 6 as a function of the annealing temperatures. The index change Δn_z between the tracks and the bulk material gradually fell from −0.022 to −0.01 when the waveguide was thermally treated. Regarding to the index change Δn_y, it was not measured until the CLWs were single mode, for the thermal treatment of 773K. At this point the measured Δn_y is −0.01 which is around a 62% of the Δn_z values (−0.016). A dramatic drop of the Δn_y is also observed at 973K and keeping stable until 1073K. Overall, these observations match well with the known anisotropy of LiNbO$_3$ and the large differences between the effects on the ordinary or extraordinary index of the crystal when subjected to laser irradiation.
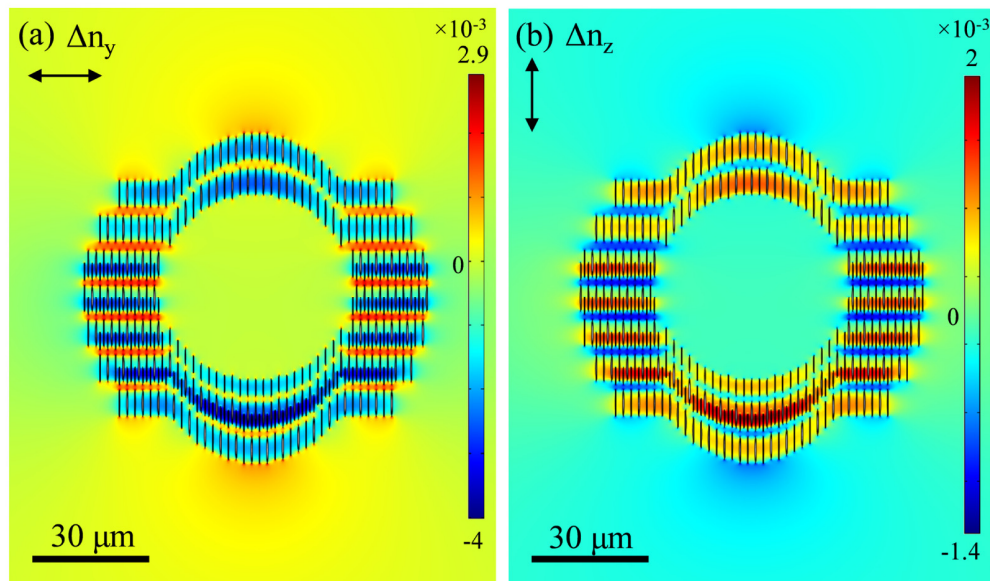

Fig. 7. Index profiles including the changes of ordinary Δn_y (a) and extraordinary Δn_z (b) indices of the waveguide 750_wg8 after thermal treatment of 773K. The refractive index changes inside tracks are $\Delta n_y = -0.01$ and $\Delta n_z = -0.016$.

3.3.3. Profile of the waveguide after 773K annealing

It is interesting to notice that although the magnitude of all the depressed-Δn tracks and the induced stress steadily dropped from the beginning to the end of the annealing steps, the waveguiding performance in terms of PLs oscillated and did not follow a simple trend, as seen on Fig. 3. To showcase the complexity and interplay between tracks and stress fields, in Fig. 7 we show the 2D computed index profiles CLW 750_wg8 after annealed at 773K. In the case of TE guiding, the Δn_y profile shows that some areas with increased index (red) come in between the vertical layers of low-index tracks, introducing a complex inhomogeneity to the cladding microstructure. This interference might not be significant, as the TE measured guided light always increased in PLs with the annealing steps. The TM index profile appears

also complicated, with an induced positive stress-optic index change (Δn_z) in the lateral sides (red regions) of the low-index tracks across the whole cladding structure.

Using these obtained index profiles, TE and TM modes are compared with the measured mode fields. As Fig. 8 shows, both simulated and measured are well-matched. The PLs also have good matching which is in order of <0.1 dB/cm error. The FEM design is obtained from the analysis of the SEM image of the cladding structure also shown.
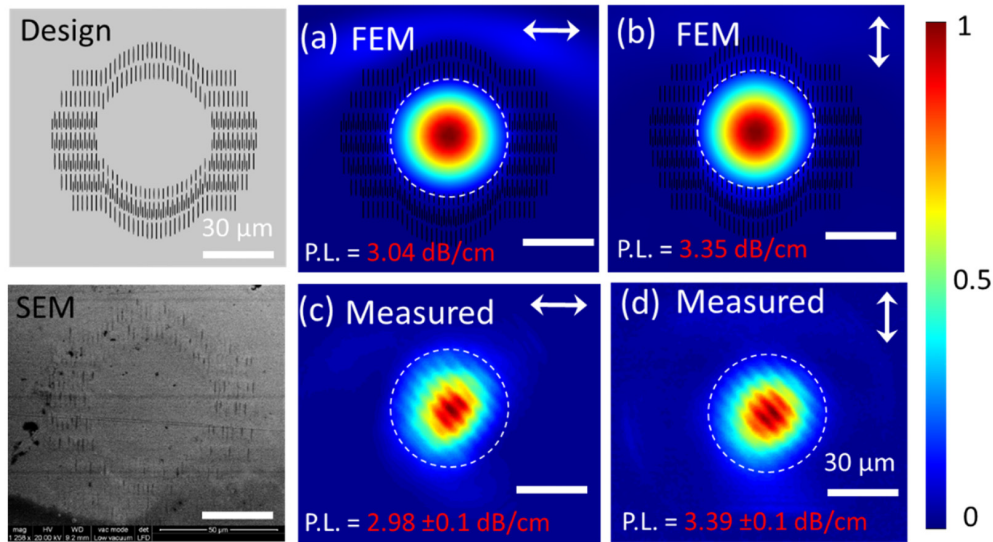

Fig. 8. Simulation and experiment of the CLW 750_wg8: Comparison of near field TE and TM modes at 3.68 μm wavelength. Interference fringes in the measured mode images are due to back-reflections in the optical guiding imaging system.

3.4 Optimal waveguide performance towards the lowest losses in both orthogonal polarizations

The section §3.1 has confirmed that low-speed laser inscription can offer low-loss waveguides even by using low levels of pulse energy. More homogenous damage tracks can be obtained when the overlapped areas are larger which significantly decreases the propagation losses at 3.68 μm in the mid-IR range. Our double ring cladding design has achieved low-loss waveguiding by using pulse energies of 1.68 μJ at scanning speed of 500 μm/s. This design and the use of laser conditions did not require a large amount of time (< 3h) to fabricate and provide a significant improvement of the waveguide. The reported CLW2R 500_wg5 with lowest losses showed multimode guiding for both TE and TM polarizations as fabricated. However, the higher order modes were shown to clean up by applying controlled thermal treatments. As studied in Section §3.3, the waveguide was measured to have single mode guiding with reasonably low losses of 1.25 dB/cm and 1.79 dB/cm for TM and TE polarized light, respectively. This is the first time (to our knowledge) that single mode guiding for both TE and TM polarizations is achieved, and with propagation losses around ~1.5 dB/cm which start to be within the range for instrumental developments.

4. Conclusions

In this work, we have designed a new double-widened cladding arrangement in search for improvements of the LiNbO$_3$ CLW performance in the mid-infrared. More specifically our goal was to achieve, for the first time to our knowledge, LiNbO$_3$ cladding waveguides for the mid-infrared being single mode, and guiding for both TE and TM orthogonal polarizations. The distinctive behavior of the waveguide under heat treatments has been explored with a

focus on optimizing the waveguide properties for both polarizations both in terms of achieving single modality and low losses. A complete set of the anisotropic $\Delta n_{y,z}$ changes of CLWs in the mid-IR has been revealed to understand the effects of the thermal annealing. Single mode guiding for TM and TE polarisations has been obtained with PLs of 1.25 dB/cm and 1.79 dB/cm, respectively. This significant improvement is of high potential for the implementation of integrated photonic devices working in the mid-IR range. This type of cladding waveguide takes advantages of maintaining the material properties (as the waveguiding core is considerably un-modified). Implementation of these cladding structures on lithium niobate which possesses high electro-optical and non-linear coefficients; opens a bright pathway for true high performance of real devices including non-linear frequency converters, interferometric spectrometers, interferometers, etc.

Funding